Integrated silicon modulator based on microring array assisted MZI

Xiangdong Li, Xue Feng,* Kaiyu Cui, Fang Liu, and Yidong Huang

Department of Electronic Engineering, Tsinghua National Laboratory for Information Science and Technology, Tsinghua University, Beijing 100084, China
x-feng@tsinghua.edu.cn

Abstract: A silicon modulator with microring array assisted MZI is experimentally demonstrated on silicon-on-insulator wafer through CMOS-compatible process. The footprint of the whole modulator is about 600 μm^2. With forward-biased current-driven p-n junction, the 3-dB modulation bandwidth is ~2GHz. Furthermore, the impact of ambient temperature is minified with the help of MZI. Within temperature range of 10 – 70 °C, the maximum divergence of modulation curve is less than ~3 dB.

OCIS codes: (200.4650) Optical interconnects; (130.4110) Modulators; (130.3990) Micro-optical devices; (120.6780) Temperature.

References and links

1. G. T. Reed, G. Mashanovich, F. Y. Gardes, and D. J. Thomson, "Silicon optical modulators," Nat. Photonics **4**(8), 518–526 (2010).
2. D. Marris-Morini, L. Vivien, G. Rasigade, J.-M. Fedeli, E. Cassan, X. Le Roux, P. Crozat, S. Maine, A. Lupu, P. Lyan, P. Rivallin, M. Halbwax, and S. Laval, "Recent progress in high-speed silicon-based optical modulators," Proc. IEEE **97**(7), 1199–1215 (2009).
3. Q. F. Xu, S. Manipatruni, B. Schmidt, J. Shakya, and M. Lipson, "12.5 Gbit/s carrier-injection-based silicon micro-ring silicon modulators," Opt. Express **15**(2), 430–436 (2007).
4. L. Chen, K. Preston, S. Manipatruni, and M. Lipson, "Integrated GHz silicon photonic interconnect with micrometer-scale modulators and detectors," Opt. Express **17**(17), 15248–15256 (2009).
5. M. R. Watts, W. A. Zortman, D. C. Trotter, R. W. Young, and A. L. Lentine, "Vertical junction silicon microdisk modulators and switches," Opt. Express **19**(22), 21989–22003 (2011).
6. D. J. Thomson, F. Y. Gardes, J. M. Fedeli, S. Zlatanovic, Y. F. Hu, B. P. P. Kuo, E. Myslivets, N. Alic, S. Radic, G. Z. Mashanovich, and G. T. Reed, "50-Gb/s silicon optical modulator," IEEE Photon. Technol. Lett. **24**(4), 234–236 (2012).
7. P. Dong, L. Chen, and Y. K. Chen, "High-speed low-voltage single-drive push-pull silicon Mach-Zehnder modulators," Opt. Express **20**(6), 6163–6169 (2012).
8. T. Y. Liow, K. W. Ang, Q. Fang, J. F. Song, Y. Z. Xiong, M. B. Yu, G. Q. Lo, and D. L. Kwong, "Silicon modulators and germanium photodetectors on SOI: monolithic integration, compatibility, and performance optimization," IEEE J. Sel. Top. Quantum Electron. **16**(1), 307–315 (2010).
9. H. C. Nguyen, Y. Sakai, M. Shinkawa, N. Ishikura, and T. Baba, "10 Gb/s operation of photonic crystal silicon optical modulators," Opt. Express **19**(14), 13000–13007 (2011).
10. A. M. Gutierrez, A. Brimont, G. Rasigade, M. Ziebell, D. Marris-Morini, J. M. Fédéli, L. Vivien, J. Marti, and P. Sanchis, "Ring-assisted Mach–Zehnder interferometer silicon modulator for enhanced performance," J. Lightwave Technol. **30**(1), 9–14 (2012).
11. X. J. Zhang, X. Feng, D. K. Zhang, and Y. D. Huang, "Compact temperature-insensitive modulator based on a silicon microring assistant Mach Zehnder interferometer," Chin. Phys. B **21**, 124203 (2012).
12. F. Shinobu, N. Ishikura, Y. Arita, T. Tamanuki, and T. Baba, "Continuously tunable slow-light device consisting of heater-controlled silicon microring array," Opt. Express **19**(14), 13557–13564 (2011).
13. S. Akiyama, T. Kurahashi, T. Baba, N. Hatori, T. Usuki, and T. Yamamoto, "1-Vpp 10-Gb/s operation of slow-light silicon Mach-Zehnder modulator in wavelength range of 1 nm," in *IEEE International Conference on Group IV Photonics*, (Beijing, China, 2010), pp. 45–47.
14. Y. Li, L. Zhang, M. Song, B. Zhang, J. Y. Yang, R. G. Beausoleil, A. E. Willner, and P. D. Dapkus, "Coupled-ring-resonator-based silicon modulator for enhanced performance," Opt. Express **16**(17), 13342–13348 (2008).
15. L. Zhang, M. Song, T. Wu, L. Zou, R. G. Beausoleil, and A. E. Willner, "Embedded ring resonators for microphotonic applications," Opt. Lett. **33**(17), 1978–1980 (2008).
16. Q. Xu, "Silicon dual-ring modulator," Opt. Express **17**(23), 20783–20793 (2009).
17. Y. Hu, X. Xiao, H. Xu, X. Li, K. Xiong, Z. Li, T. Chu, Y. Yu, and J. Yu, "High-speed silicon modulator based on cascaded microring resonators," Opt. Express **20**(14), 15079–15085 (2012).

#206524 - $15.00 USD Received 17 Feb 2014; revised 19 Apr 2014; accepted 20 Apr 2014; published 24 Apr 2014

18. J. E. Heebner, V. Wong, A. Schweinsberg, R. W. Boyd, and D. J. Jackson, "Optical transmission characteristics of fiber ring resonators," IEEE J. Quantum Electron. **40**(6), 726–730 (2004).
19. L. Zhang, Y. C. Li, J. Y. Yang, M. P. Song, R. G. Beausoleil, and A. E. Willner, "Silicon-based microring resonator modulators for intensity modulation," IEEE J. Sel. Top. Quantum Electron. **16**(1), 149–158 (2010).

1. Introduction

Optical interconnection is considered as a promising solution for future high-performance multi-core processors with the attractive prospect of integration with complementary metal-oxide-semiconductor (CMOS) electronics on the same silicon substrate. Silicon optical modulator is a major workhorse in such an optical interconnect system. Till now, the reported silicon modulators are dominantly based on two approaches of the Mach-Zehnder interferometer (MZI) and resonant cavity [1, 2]. For modulators based on resonant cavity, *e.g.* microring or disk, the narrow operating spectrum (typically ~0.1 nm) and temperature sensitivity are the main limitations due to the resonant nature [3–5]. On the other side, the temperature stability of a MZI modulator is very outstanding due to the symmetrical structure, while the device footprint is relatively large (10^3 – 10^5 μm^2) [6–8]. One way to overcome it is to introduce slow-light structures so that the phase-shifter efficiency can be increased to achieve shorter device length [9, 10]. Besides photonic crystal waveguide (PCW), which is a typical one of these structures [9], microring array could also act as a slow-light structure [11, 12]. Actually, there have been several reports about the enhanced performance of modulators by introducing more than one ring [13–17]. Therefore, ring array assisted MZI silicon modulator may open up a new and practical approach for integrated silicon modulator.

In this paper, we experimentally demonstrate a microring array assisted MZI modulator with CMOS-compatible fabrication processes. Three microrings operating at over-coupled state are coupled with each arm of MZI. The device footprint is about 600 μm^2. Based on forward-biased current-driven p-n junction, the modulation efficiency is rather high while voltage length product is estimated as low as $V_\pi L < 6.63 \times 10^{-3}$ V·cm at room temperature (20 °C). The temperature stability is also tested and it possesses good temperature insensitivity within 10 to 70 °C with maximum divergence of < 3 dB. Finally, the 3-dB bandwidth of measured frequency response is about 2 GHz. A square wave signal, whose rising edge is about 1 ns and peak voltage is 350 mV, is also modulated.

2. Design and fabrication

Figure 1(a) is the layout of our proposed modulator. Here, a balanced MZI is adopted while there is a microring array coupled with each arm. In our previous work [11], it has been presented that the operating principle relies on a balanced MZI and over-coupled microring array. For microrings operating at the over-coupled state, there will be a wide wavelength range of linear phase response so that the arm length of MZI could be reduced and more compact device footprint could be achieved. Actually, a single microring could serve as a slow-light delay line. But the delay bandwidth is narrow so that it is very sensitive to ambient temperature variation. As shown in [12], one way to achieve wide delay bandwidth is to employ the microring array in which the diameter of each microring gradually varies. And the delay bandwidth of microring array is determined by the interval of resonant wavelengths among different rings. Theoretically, better temperature stability could be achieved with broader delay bandwidth and more microrings in succession. However, increasing the number of rings also leads to longer device length and more sensitivity to the fabricating fluctuation. As a tradeoff between device footprint and temperature stability, the ring number is chosen as three in this work. The detailed discussion could be found in our previous work [11].

#206524 - $15.00 USD Received 17 Feb 2014; revised 19 Apr 2014; accepted 20 Apr 2014; published 24 Apr 2014

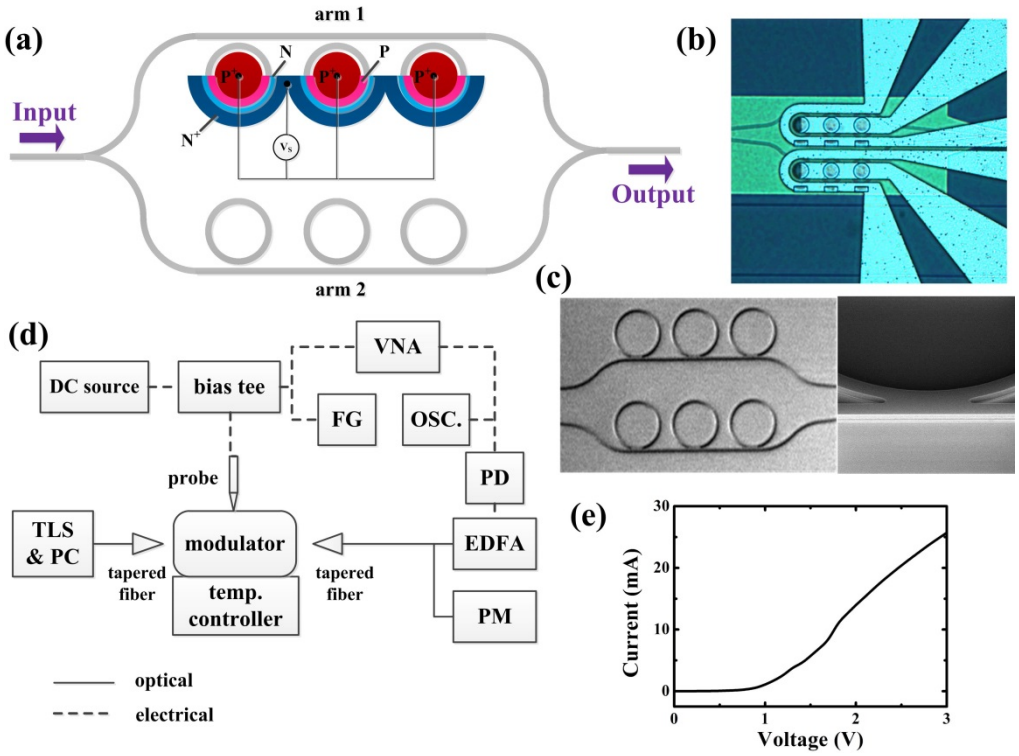

Fig. 1. (a) The structure of microring array assisted MZI silicon modulator; (b) microscopic image of the fabricated modulator with the electrodes; (c) scanning electron microscope (SEM) images of the sample after etching and without ion implantation; (d) schematic measurement system of the modulator; (e) the *I-V* curve of the p-n junction.

The proposed modulator is fabricated by the photonics prototyping service of the Institute of Microelectronics (IME) in Singapore. The silicon-on-insulator (SOI) wafer with a 220-nm-thick top silicon layer and a 2-μm-thick buried oxide layer is used. The pattern of the modulator is defined with a 248 nm deep UV lithography. All the waveguides are etched with inductively coupled plasma reactive ion etch (ICP-RIE). All waveguides are silicon rib waveguides with width of 450 nm, height of 220 nm, and a slab layer with thickness of 60 nm. The arm length of MZI is designed as L = 30 μm and the diameters of three rings are D = 9.98 μm, 10 μm and 10.02 μm, respectively. The distance between the two microrings is 3 μm. Each microring with one arm incorporates a p-n junction, consisting of moderately-doped p and n, as well as highly-doped p^+ and n^+ regions. The doping level is in the range of 10^{17} cm^{-3} and the detailed concentration distribution of p-n junction could be found in [8]. On top of waveguides, a SiO_2 cladding layer is deposited. Then, an electrode is formed and contacted with p-type and n-type doping region through etched windows on the cladding layer as shown in Fig. 1(b). The electrode contacted with p-n junction is 50 nm/0.75 μm/25 nm TaN/Al/TaN and the electrode on the cladding layer is 2 μm/25 nm Al/TaN. The widths of electrode contacted with P-type doping region and N-type doping region are 7 μm and 4 μm, respectively. Additionally, an inverse taper is adopted at the end of input and output waveguide to effectively couple with fibers in the measurement. According to the SEM photo, the device footprint of the whole modulator is about 600 μm^2.

According to our simulation [11], this arrangement is enough for stable operation with the temperature span of 130 °C and the gap distance between the arm and the corresponding microring should be 0 – 30 nm to ensure that all microrings operate at much over-coupled state while attenuation coefficient of fabricated Si waveguide is ~2 dB/cm. However, after

#206524 - $15.00 USD Received 17 Feb 2014; revised 19 Apr 2014; accepted 20 Apr 2014; published 24 Apr 2014

doping, the waveguide loss would increase due to carrier absorption so that the gap distance should be narrower than 28 nm [11] and thus it is set as 20 nm in lithography mask. Actually, such narrow gap cannot be fabricated with existing lithography technology. As shown in the SEM photograph after etching (Fig. 1(c)), the rings conglutinate the arm of MZI. In order to evaluate the impact of such conglutination, some simulations have been carried out with finite difference time domain (FDTD) method and the results are shown in Fig. 2. Here, only one microring with D = 10 μm and gap distance of 20 nm is concerned with and without conglutination according to the SEM photograph. Figure 2(a) is the calculated transmission spectrum around 1550 nm, which is the concerned operating wavelength of our modulator. It could be found that the conglutination would increase the insertion loss (< 3 dB) while the spectrum is still very flat. In order to reveal the operating state of microring, the spectra of transmission and phase shift around the resonant wavelength are also calculated. Figure 2(b) and 2(c) are the results with and without conglutination, respectively. Comparing them, it could be found that the resonant wavelength (closest to 1550 nm) is varies from 1535.3 nm to 1538.5 nm due to conglutination, but the phase shift around resonance is also slowly varied so that both the two rings are working at over-coupled state. These simulation results indicate that there is little influence on operating state of microring with conglutination while the insertion loss would increase (< 3 dB@1550 nm).

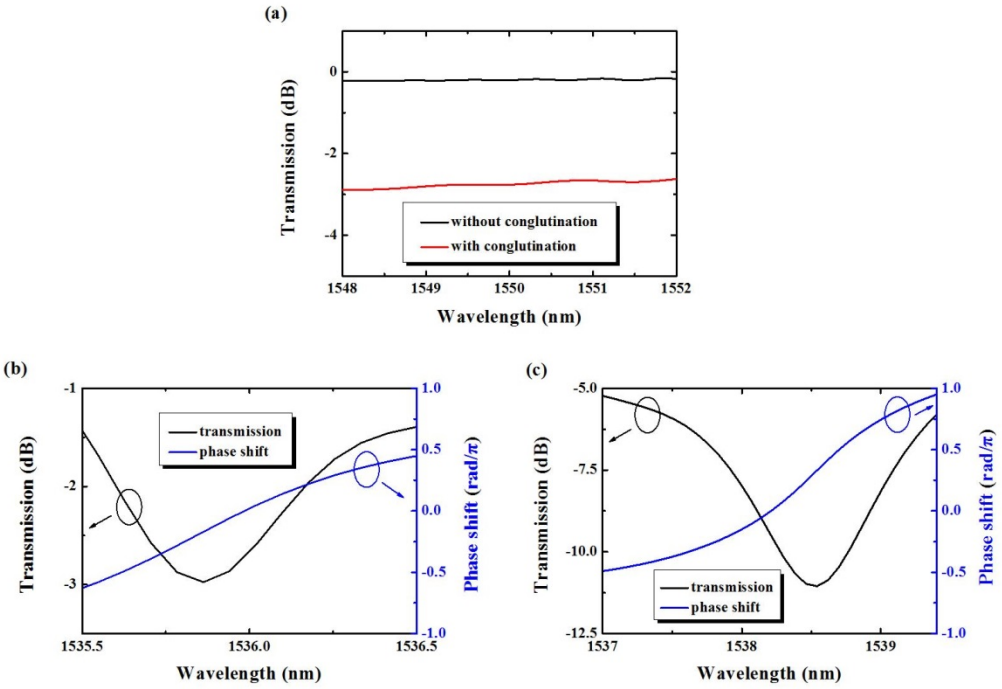

Fig. 2. (a) The transmission spectrum without (solid) and with (dashed) conglutination at 1548 – 1552nm; the transmission and phase shift spectrum without (b) and with (c) conglutination at the resonant wavelength. Here, only one microring with D = 10 μm and gap distance of 20 nm is calculated with FDTD method.

The prepared device samples are characterized with a setup as Fig. 1(d), including a tunable laser source (TLS), a polarization controller (PC, Agilent 11896A) and a power meter (PM, Agilent 81624A). The output power of TLS is set as a constant value of 0.5 mW (–3 dBm). Single-mode lensed optical fibers, mounted on a computer-controlled alignment stage, are used to couple light in and out. A temperature controller with a precision current source (ILX Lightwave LDX-3412) is employed to set the ambient temperature with the range of 10

#206524 - $15.00 USD Received 17 Feb 2014; revised 19 Apr 2014; accepted 20 Apr 2014; published 24 Apr 2014

– 70 °C. In the experiment, the time interval between different temperatures is more than ten minutes, and each value is repeatedly measured with a thermometer to ensure thermal equivalence. A direct current (DC) source (Agilent B2901A) is used to measure the *I-V* curve and the results are shown in Fig. 1(e). The turn-on voltage is about 0.9 V and the resistance is 70 – 80 Ω. To obtain modulation characteristics, the microwave signal is generated from a function generator (FG) or a 40-G vector network analyzer (VNA, Agilent Technologies E8363B), combined with a suitable DC signal through a bias tee. Additionally, a high-frequency ground-signal-ground (GSG) probe (Cascade Microtech FF23H ACP50-AW-GSG-150) is used to connect with the electrodes. The output light is detected by a photo detector (PD, U2T XPDV2120R), and corresponding waveform and microwave signal response spectrum are measured by an oscilloscope (Agilent infiniium 54833A) and VNA, respectively.

3. Measurements and results

The device is firstly tested without driving voltage. Figure 3(a) shows the output spectra (from 1548 to 1552 nm) at varied temperatures from 10 to 70 °C. Here, the operating wavelength is considered as 1550 nm and it could be found that the maximum power variation is about 3.4 dB (from –21.7 to –25.1 dBm). This result is different to the expectation of our previous simulations in [11]. Since the lengths of two MZI arms are identical, we attribute such deviation to the fabrication error of the microrings and some simulations have been carried out with the method in [18] to reveal it. Firstly, the two MZI arms and corresponding rings on each arm are considered as symmetrical. The diameters of rings are the same as designed values (D = 9.98 μm, 10 μm and 10.02 μm) while the length of each arm, transmission coefficient of each coupler and transmission factor of each ring are identically set as 30 μm, 0.4 and 0.9, respectively. The calculated results are shown in Fig. 3(b) while the upper figure is the power transmission of the modulator with varied temperatures from 10 to 70 °C and the lower one is the phase delay difference between the two MZI arms ($\Delta\phi = \phi_{arm2} - \phi_{arm1}$). In the lower figure, red dash and black solid line are calculated with the refractive index difference of Δn = 0 and Δn = 0.005 applied on the microring array of one MZI arm. It could be found that the modulator could operate within the wavelength range of 1548 – 1552 nm. In such range the transmission loss only varies < 5 dB with the varied temperatures of 10 – 70 °C. Meanwhile, with Δn = 0.005 applied on the microring array of one MZI arm, the $\Delta\phi$ of about 0.4π – 0.8π would be introduced within the range of 1548 – 1552 nm. Specifically, $\Delta\phi$ is ~0.6π at 1550 nm, which is equal to the length of ~100 μm for rib waveguide with the same Δn. Since the arm length of our proposed modulator is only 30 μm, there is an enhanced factor of ~3 attributed by the slow light effect of the microring array, which is the foundation of this work. However, for the practical device, fabrication errors could not be avoided. Especially, the perimeter variation of the rings would introduce more complicated temperature evolution of output spectrum. Thus, the transmission spectra are also calculated with random diameter variation (as shown in Table 1) added on each ring of one arm. In Fig. 3(c), the calculated power transmission and $\Delta\phi$ spectra are shown in the upper and lower figure, respectively. It can be seen that there are several peaks and valleys in the transmission spectra. For a clear comparison with the experimental results, the enlarged transmission spectra within the range of 1548 – 1552 nm are shown in Fig. 3(d). It could be found that the spectrum shape is very similar to the measured one. Moreover, as shown by the arrows in Fig. 3(d), the transmission spectrum would exhibit redshift with increasing temperature, which is also consistent with the experimental result. For the $\Delta\phi$, it is found that additional phase delay would be introduced even with Δn = 0 as shown with red dash line in the lower figure of Fig. 3(c). That is the reason why the transmission spectrum is deteriorated. As a result of asymmetric microring array, the operating wavelength is not arbitrary and should be the one with low insertion loss, e.g. 1548 nm, 1550 nm and 1552 nm as shown in Fig. 3(a) and the wavelength range is reduced to

#206524 - $15.00 USD Received 17 Feb 2014; revised 19 Apr 2014; accepted 20 Apr 2014; published 24 Apr 2014

~1nm (1549.4 – 1550.4 nm). It should be mentioned that $\Delta\phi$ induced by Δn is also $0.5\pi - 0.6\pi$ within this wavelength range (shadow in the lower figure of Fig. 3(c)), which means that the slow light effect of microring array is also acting. All the results mentioned indicate that the fabrication error of microrings would have little influence on the temperature stability and slow light effect but have a significant impact on the operating wavelength range. For our fabricated device, the wavelength range is about 1 nm around 1550nm that could sustain 40 GHz modulation bandwidth with proper alignment of optical carrier. If larger modulation bandwidth is desired, higher precise fabrication is demanded. Additionally, as the input power is –3 dBm, the total attenuation is about 19 dB before PM, which consists of the fiber coupling loss and insertion loss. Taking a silicon rib waveguide as reference, the insertion loss of the modulator is estimated as 7 – 9 dB at 1550 nm for four samples.

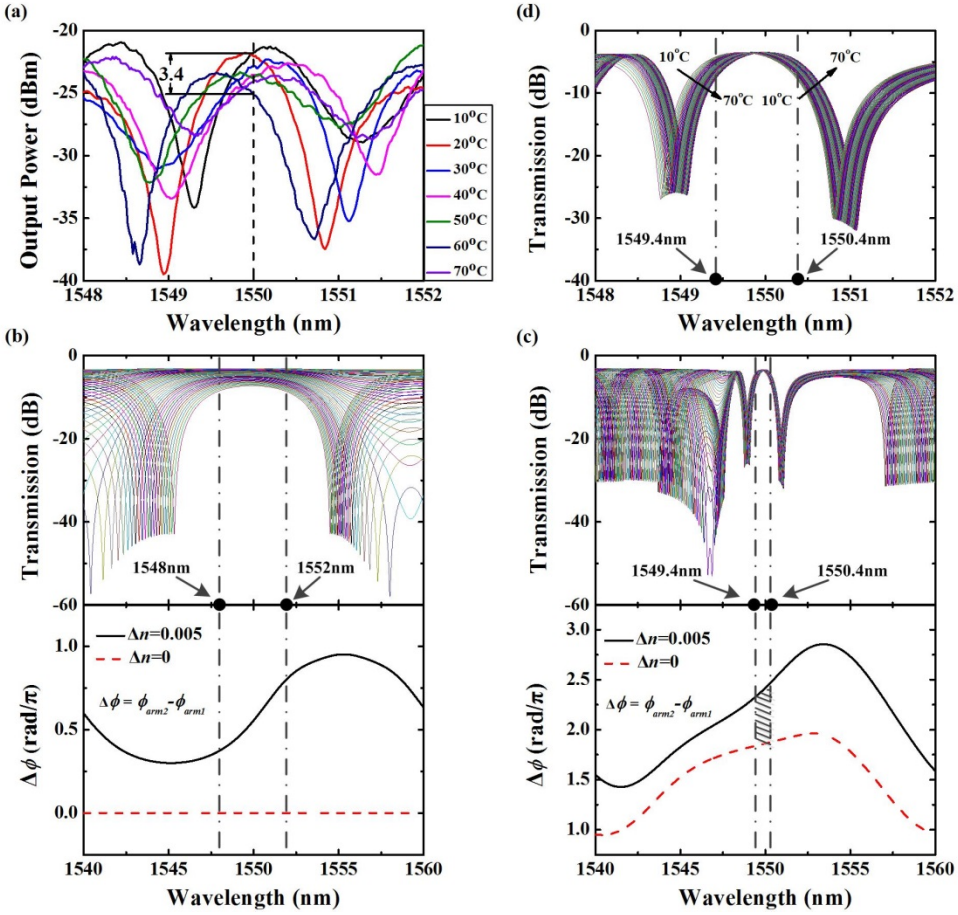

Fig. 3. (a) Measured output spectra at different temperatures; transmission and $\Delta\phi$ spectra of symmetrical (b) and asymmetrical (c) structure at different temperatures in wavelength range of 1540 – 1560nm; (d) enlarged transmission spectra for asymmetrical structure within the range of 1548 – 1552 nm.

Table 1. The diameters of each ring for calculating Fig. 3(b)

	ring 1	ring 2	ring 3
arm 1	9.90 μm	10.00 μm	10.20 μm
arm 2	9.98 μm	10.02 μm	10.04 μm

Next, the electrooptic efficiency is measured at room temperature (20 °C). In order to exclude the thermooptic effect, which is too slow for high speed modulation, a 10 MHz

#206524 - $15.00 USD Received 17 Feb 2014; revised 19 Apr 2014; accepted 20 Apr 2014; published 24 Apr 2014

sinusoidal electrical signal is applied. Figure 4 shows the oscilloscope traces of the detected signals at different bias voltages. In the experiment, the drive amplitude of the sinusoidal signal (peak-to-peak value of voltage, V_{pp}) increases until the peaks or troughs of the detected signal begin to overturn. Without a DC bias, the V_{pp} to achieve overturn is 2.21 V as shown in Fig. 4(a). Taking turn-on voltage of p-n junction (0.9 V) into consideration, V_{pp} = 2.21 V should be larger than half wave voltage V_π. Thus as a conservative estimation, the half wave voltage of our modulator should be $V_\pi < 2.21$ V. Figure 4(b) shows the results with DC bias of 1.1 V. In this case, a complete sinusoidal signal is detected, and the V_{pp} to achieve overturn is 0.428 V and this value could be treated as $V_\pi = 0.428$ V. Although this value is not strict to present the half voltage since the thermal effect could be introduced by the DC bias, it offers another evidence of $V_\pi < 2.21$ V. By multiplying $V_\pi < 2.21$ V with the length of each arm (L), the figure of merit $V_\pi L$ is calculated as $V_\pi L < 6.63 \times 10^{-3}$ V·cm. As mentioned above, there is a factor of ~3 to reduce the arm length due to the slow light effect so that the modulation efficiency is improved. Meanwhile, it should be noticed that the overall efficiency is also related to the electrical and carrier transport characteristics. However, it is not easy to estimate the accurate value since the exact doping level and profile of p-n junction employed are unknown. Comparing the $V_\pi L$ of our device with others and taking the enhanced factor into account, we believe that both the microring array and p-n junction play a role in improving the overall efficiency.

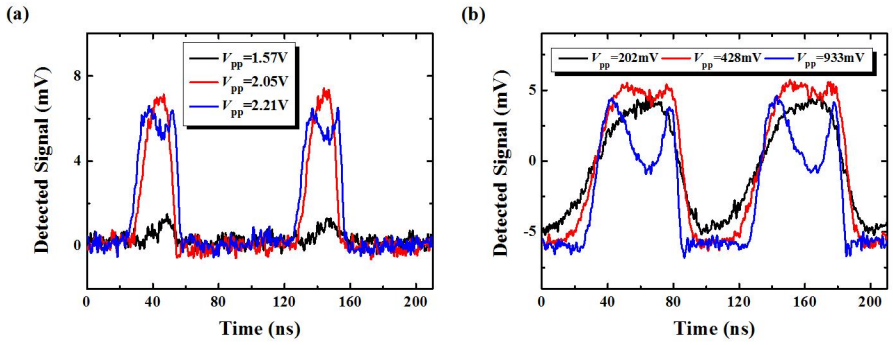

Fig. 4. The oscilloscope traces of the detected signals. (a) The DC bias is 0 V; (b) the DC bias is 1.1 V.

Furthermore, the microwave frequency response is also measured at the wavelength of 1550 nm. The DC bias is set as 1.1 V and the signal power is from –10 to 16 dBm, which is limited by the VNA. Figure 5(a) is the measured results with the signal power of 12 dBm. The 3-dB bandwidth is about 2 GHz. Such modulation bandwidth could sustain transmission data rate higher than 1 Gb/s with non-return-to-zero signal and if pre-emphasis of driving signal is employed, higher data rate could be achieved [9]. Figure 5(b) shows the bandwidths under different signal powers. It could be found that higher signal power is better, which is similar to an over-coupled ring modulator as in [19]. In addition, a square wave signal with rising edge of 200 ps and peak voltage of 350 mV is modulated. The driving signal (black and dashed) and detected signal (blue and real) are shown in Fig. 5(c). Limited by the bandwidth of the oscilloscope, the rising edges of the driving signal and detected signal are ~1 ns. It should be mentioned that due to the forward-biased p-n junction, the modulation bandwidth is lower than those reported in recent years. A straightforward way to improve it is to employ other carrier injection structures, *e.g.* depletion of a horizontal p-n junction and reverse-biased p–n junction [1]. It should be mentioned that employing high speed p-n junction may increase the half wave voltage V_π and leads to the deterioration of the overall modulation efficiency.

#206524 - $15.00 USD Received 17 Feb 2014; revised 19 Apr 2014; accepted 20 Apr 2014; published 24 Apr 2014

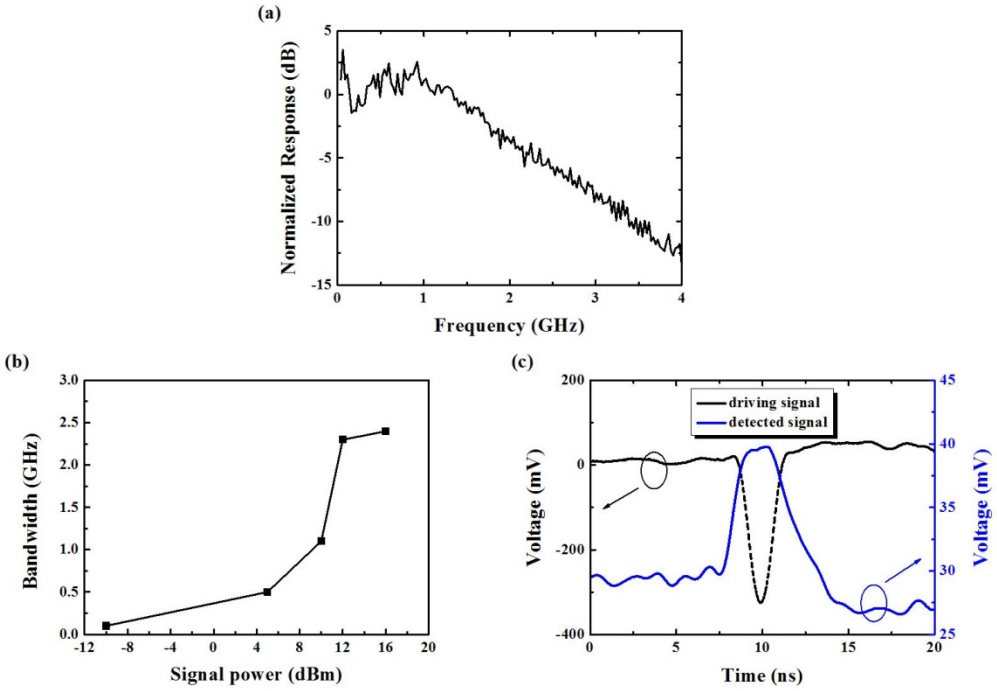

Fig. 5. (a) Normalized microwave frequency response of the modulator; (b) the bandwidths under different signal powers; (c) the modulated square wave signal.

Finally, the modulation curves are measured with varied temperatures from 10 to 70 °C at the wavelength of 1550 nm. The normalized results are shown in Fig. 6. For the modulation curve, the maximum divergence is about 3 dB within the range of 0 to 2 V. Such variation is nearly equal to that without driving voltage (Fig. 3(a)). Thus, we believe that it is mainly due to the asymmetrical ring arrays and could be further reduced with improving fabrication technology. Such experimental results indicate that our proposed modulator possesses good temperature stability within 10 to 70 °C. It should be mentioned that the measurements only carried out within such range are limited by temperature controller.

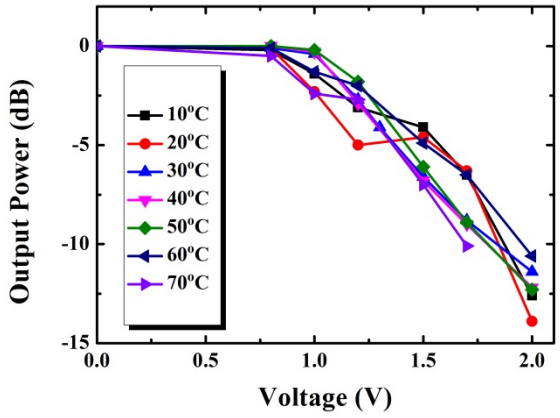

Fig. 6. Modulation curves at different temperature.

#206524 - $15.00 USD Received 17 Feb 2014; revised 19 Apr 2014; accepted 20 Apr 2014; published 24 Apr 2014

4. Conclusions

In this paper, a silicon modulator is experimentally demonstrated on SOI wafer through CMOS-compatible fabrication processes. Due to the symmetrical structure of MZI, the maximum divergence of modulation curves is only 3 dB within the temperature range of 10 – 70 °C. Meanwhile, with the help of over-coupled microring array, the arm length of MZI is only 30 μm and consequently the corresponding voltage length product is as low as $V_{\pi}L < 6.63 \times 10^{-3}$ V·cm. The measured 3 dB modulation bandwidth is ~2 GHz.

Acknowledgments

This work was supported by the National Basic Research Program of China (No. 2011CBA00608, 2011CBA00303, 2011CB301803, and 2010CB327405), the National Natural Science Foundation of China (Grant No. 61307068, 61036010, 61036011, and 61321004). The authors would like to thank Dr. Wei Zhang, Mr. D. K. Zhang, Mr. Y. Z. Li, and Mr. Q. Zhao for valuable discussions and helpful comments. The authors also thank the Institute of Microelectronics, Singapore for device fabrication.